ISSN: 1410-8917
Jurnal Kimia Sains & Aplikasi
e-ISSN: 2597-9914

Jurnal Kimia Sains dan Aplikasi 27 (4) (2024): 174-181

Jurnal Kimia Sains dan Aplikasi
Journal of Scientific and Applied Chemistry

Journal homepage: http://ejournal.undip.ac.id/index.php/ksa

Synthesis and Characterization of Fluorapatite-Copper(II) Oxide with Sol-Gel Method as an Antibacterial Biomaterial

Manasye Erlangga [1], Charlena [1,*], Irma Herawati Suparto [1]

[1] Department of Chemistry, Faculty of Mathematics and Natural Sciences, IPB University, Bogor, West Java, Indonesia

* Corresponding author: charlena@apps.ipb.ac.id

https://doi.org/10.14710/jksa.27.4.174-181

Article Info

Article history:

Received: 06th December 2023
Revised: 11th April 2024
Accepted: 16th April 2024
Online: 30th April 2024

Keywords:
Antibacterial; fluorapatite-copper(II) oxide; sintering; sol- gel

Abstract

One of the calcium phosphate compounds that can be used as an antibacterial material for coating dental implants is fluorapatite (FAp). This research aims to synthesize FAp at three different sintering temperatures (600, 800, and 1000°C), copper(II) oxide (CuO), and fluorapatite-copper(II) oxide (FAp-CuO) using the sol-gel method, and test the antibacterial properties of the synthesized products. The sol-gel technique proved successful in synthesizing FAp, with optimal results observed at a sintering temperature of 1000°C, achieving a crystallinity level of 90%. Analyses conducted using X-ray diffractometer, Fourier-transform infrared spectrometer, and scanning electron microscope-energy dispersive X-ray spectrometer revealed FAp as the dominating phase, exhibiting Ca/P and P/F ratios of 1.84 and 4.67, respectively. In FAp-CuO, replacing Ca^{2+} with Cu^{2+} ions lowered the average crystallite size, crystallinity, and Ca/P ratio. FAp, CuO, and FAp-CuO all displayed antibacterial activities against *S. aureus* and *E. coli*, with FAp-CuO having the maximum average inhibitory zone diameters of 0.243 and 1.397 mm, respectively.

1. Introduction

Biomaterials are synthetic materials designed to replace body parts through interactions with living tissues and are inert to these living tissues [1]. Biomaterials also have properties and characteristics acceptable to body tissues, making them commonly utilized in various medical applications such as bone implants, dental fillings, catheters, heart valve replacements, and drug delivery systems [2]. Fluorapatite ($Ca_{10}(PO_4)_6F_2$) or FAp is a calcium phosphate biomaterial like hydroxyapatite ($Ca_{10}(PO_4)_6(OH)_2$) or HAp, but hydroxide ions (OH^-) are replaced by fluoride ions (F^-). Replacement of OH^- by F^- increases biodegradability and bioactivity [3] while reducing ion solubility and reactivity [4].

Fluorapatite can be synthesized through various methods, including chemical precipitation with a sintering temperature of up to 1200°C [4], the sol-gel method followed by sintering at 550°C [3], and ball-milling with a milling duration ranging from 24 to 48 hours [5]. All three methods have been reported to produce crystalline FAp. In this study, the sol-gel method was employed. This choice was motivated by several factors: its capacity to generate high-quality products with uniform particle distribution, its suitability for low-temperature applications, and its cost-effectiveness [6]. The sol-gel method is categorized as a bottom-up synthesis method, which entails irreversible chemical reactions to produce the final product [7].

In this research, fluorapatite was synthesized using biogenic waste, specifically sourced from the golden snail shell (*Pomacea canaliculata*). The selection of the golden snail shell as the raw material for FAp synthesis was based on its high calcium carbonate ($CaCO_3$) content, which amounts to 99% [8]. This surpasses the calcium carbonate content found in other biogenic wastes, such as chicken eggshells (41%), duck eggshells (40%), and quail eggshells (38%) [9]. Fluoride ions can be obtained by adding ammonium fluoride (NH_4F), sodium fluoride (NaF), or calcium fluoride (CaF_2), which play important roles in the formation of tooth enamel [4, 10].

Fluorapatite has potential as an antibacterial agent, and its antibacterial properties are currently being explored. This antibacterial property is related to the

ability of FAp to prevent bacterial infection when applied as a dental implant coating material. Previous research conducted by Shanmugam and Gopal [10] stated that FAp can reduce the growth of *S. aureus* and *E. coli* bacteria by 67% and 60%, respectively. The antibacterial effect of FAp is attributed to the release of fluoride ions (F^-), which interfere with cellular metabolic processes, leading to the deactivation of bacterial cells. This mechanism indicates that FAp exhibits bacteriostatic properties, implying that its effectiveness is not as potent as that of other bactericidal antibacterial agents [11].

One of the bactericidal materials that can enhance the antibacterial properties of FAp is copper(II) oxide (CuO). Copper(II) oxide is a transition metal oxide with a monoclinic crystal structure and several interesting characteristics. These characteristics include thermal conductivity, photovoltaic, high stability, and antibacterial activity. This makes CuO widely applied in various fields, such as active catalysts, gas sensors, high-efficiency heat-conducting materials, magnetic recording media, and solar cells. The selection of CuO is based on its excellent antibacterial properties [12]. It has been reported to increase the reduction percentage of bacterial cells to 98% when combined with FAp [10]. These results are due to the ability of copper ions to interact with bacterial cell membranes and cause bacterial cells to die [13, 14]. The mechanism of the antibacterial properties of CuO involves Cu^{2+} ions, which interact with sulfhydryl groups in cell proteins and trigger oxidative stress that inhibits the bacteria [13].

This research aims to synthesize FAp, CuO, and FAp-CuO using the sol-gel method, determine the effect of sintering temperature variations on the FAp synthesis, and test the antibacterial activity of the synthesized products. This research is expected to provide information about sintering temperature on the FAp synthesis and to obtain high-crystalline FAp. The high-crystalline FAp can be combined with CuO via the sol-gel method and is expected to have better antibacterial properties against Gram-positive and Gram-negative bacteria.

2. Experimental

2.1. Materials

$(NH_4)_2HPO_4$ (Merck), NH_4F (Merck), ethanol (analytical reagent) (Merck), distilled water, NaOH pellets (Merck), $CuCl_2.2H_2O$ (Merck), dimethyl sulfoxide (DMSO) (Merck), Müller-Hinton agar, chloramphenicol, *Staphylococcus aureus* ATCC 6538, and *Escherichia coli* ATCC 8739 bacterial cultures.

2.2. Preparation of $Ca(OH)_2$ from Golden Snail Shells

The previously collected golden snail shells were boiled, cleaned, and dried under the sun. The dried golden snail shells were then crushed using a mortar and blender to obtain a powder of calcium carbonate ($CaCO_3$) and sifted through a 100-mesh sieve. The obtained $CaCO_3$ powder was then calcined in a furnace at 1000°C for 6 hours to convert $CaCO_3$ into calcium oxide (CaO) and release CO_2. Subsequently, CaO powder was allowed to come into contact with moisture in the air to form $Ca(OH)_2$. The formed $Ca(OH)_2$ powder was analyzed for its calcium contents using an atomic absorption spectrometer (AAS) PerkinElmer PinAAcle 900T flame-type instrument (λ = 422.7 nm). The conversion reaction of CaO to $Ca(OH)_2$ is described by chemical Equation (1).

$$CaO + H_2O \rightarrow Ca(OH)_2 \quad (1)$$

2.3. Synthesis of Fluorapatite

$(NH_4)_2HPO_4$ or DAP was used as a source of phosphate and weighed 6.603 g (50 mmol). Furthermore, DAP was mixed with 50 mL of ethanol to make a DAP suspension. The $Ca(OH)_2$ solid produced in the previous step was weighed 6.1868 g (83.5 mmol) and mixed with 50 mL ethanol to make $Ca(OH)_2$ suspension. NH_4F was used as a fluorine source, and 0.6185 g (16.7 mmol) was weighed and then mixed into the $Ca(OH)_2$ suspension. The DAP suspension was mixed slowly with the CaF_2 suspension from the previous step with constant stirring. Furthermore, the resulting reaction mixture was allowed to stand at room temperature and then dried in an oven at 120°C for 8 hours. The synthesis process was continued by sintering the dry FAp powder at 600, 800, and 1000°C for 3 hours. The product of the sintering results was cooled in a desiccator and ground using a mortar and pestle. The reaction of the FAp synthesis process is described by Equation (2) [15].

$$10Ca(OH)_2 + 6(NH_4)_2HPO_4 + 2NH_4F \rightarrow Ca_{10}(PO_4)_6F_2 + 14NH_4OH + 6H_2O \quad (2)$$

2.4. Synthesis of Copper(II) Oxide

The synthesis of CuO in this study involved two main ingredients, copper(II) chloride dihydrate ($CuCl_2.2H_2O$) and NaOH, with distilled water as the solvent. The compound $CuCl_2.2H_2O$ is a source of Cu^{2+} ions, while NaOH is a precipitating agent [16]. $CuCl_2.2H_2O$ was weighed 8.524 g (50 mmol) and dissolved in 50 mL of distilled water. Next, 4 g (100 mmol) NaOH was weighed and dissolved in 50 mL of distilled water. The 2 M NaOH solution was mixed slowly into the $CuCl_2.2H_2O$ solution with constant stirring. The reaction solution was allowed to stand for a few moments until two layers were formed. The top layer was separated, and the bottom layer was centrifuged at 5000 rpm for 20 minutes. The supernatant liquid was separated, and the solid sample was washed with distilled water two to three times to obtain $Cu(OH)_2$ solid. The $Cu(OH)_2$ solid was then dried in an oven at 120°C for 8 hours. The synthesis ended with sintering the product in a furnace at 800°C for 3 hours and then cooling it down to grind it using a mortar and pestle. The chemical reaction of CuO synthesis occurs according to Equations (3) and (4) [16].

$$CuCl_2.2H_2O + 2NaOH \rightarrow Cu(OH)_2 + 2NaCl + 2H_2O \quad (3)$$

$$Cu(OH)_2 \rightarrow CuO + H_2O \quad (4)$$

2.5. Synthesis of Fluorapatite-Copper(II) Oxide

The produced FAp and CuO were mixed with a 1:1 mole ratio. The mixing process was accompanied by constant stirring until FAp-CuO suspension was obtained. After that, the reaction product was dried in an oven at 120°C for 8 hours and sintered in a furnace at 800°C for 3 hours.

2.6. Calculation of Fluorapatite and Copper(II) Oxide Yield

Equations (2) for the synthesis of FAp and Equations (3) and (4) for the synthesis of CuO were employed in the calculation of the product yield. The yield was determined based on the ratio between the actual weight of the synthesized product and its theoretical weight. The yields of FAp and CuO were calculated using Equations (5) and (6), respectively.

$$\text{FAp yield} = \frac{\text{FAp actual weight}}{\text{FAp theoretical weight}} \times 100\% \quad (5)$$

$$\text{CuO yield} = \frac{\text{CuO actual weight}}{\text{CuO theoretical weight}} \times 100\% \quad (6)$$

2.7. Characterization Techniques

$Ca(OH)_2$, FAp, CuO, and FAp-CuO samples were characterized using Bruker D8 Advance XRD at 2θ 10-90°. The diffraction pattern obtained was then compared with the reference diffraction pattern from the crystallography open database (COD) using QualX 2.0 software. Furthermore, the crystal structures of FAp and CuO were elucidated using a crystallography information file (CIF) with the .cif extension obtained from COD. The elucidation process involved Mercury 2022.1.0 (Build 343014) software, copyrighted by Cambridge Crystallographic Data Center (CCDC) 2001-2022 Cambridge, UK. The obtained diffractogram was further used to calculate the crystallinity degree (CD) and crystallite size based on Equation (7) and Scherrer Equation (8).

$$\text{Crystallinity degree} = \frac{\text{Total area of crystalline peaks}}{\text{Total area of diffractogram}} \times 100\% \quad (7)$$

$$D = \frac{K\lambda}{\beta \cos\theta} \quad (8)$$

Where D is crystallite size (nm), K is Scherrer constant (0.94), λ is Cu K_α X-ray wavelength (0.15406 nm), β is Full Width at Half Maximum (rad), θ is diffraction angle (°).

FAp, CuO, and FAp-CuO samples were characterized using the PerkinElmer Spectrum One FTIR spectrometer to determine the presence of functional groups. The sample was mixed with 1 g of KBr and formed into pellets. The sample pellets were then measured in the 4000-400 cm^{-1} wavenumber range.

The FAp and FAp-CuO samples were characterized using a ThermoFisher Scientific scanning electron microscope with energy dispersive X-ray analyzer (SEM-EDX) instrument to determine the morphology and particle size as well as the content of calcium, phosphorus, fluorine, copper, and oxygen. The magnifications applied were 15,000 and 25,000×. Furthermore, the EDX spectrum obtained was utilized to calculate the Ca/P ratio based on Equation (9).

$$\text{Ca/P ratio} = \frac{\text{Atomic percentage of Ca}}{\text{Atomic percentage of P}} \quad (9)$$

2.8. Antibacterial Experiment

The antibacterial activity of FAp, CuO, and FAp-CuO (0.2 mg/mL) was tested using the Kirby-Bauer agar disk diffusion method with three replications. Chloramphenicol and DMSO were used as positive and negative controls, respectively. *S. aureus* ATCC 6538 and *E. coli* ATCC 8739 bacterial suspensions were prepared and aseptically spread evenly onto the surface of Müller-Hinton agar (MHA). Sterile paper discs containing FAp, CuO, and FAp-CuO samples were attached to the surface of the MHA and then incubated at 37°C for 24 hours. The inhibition zone formed around the disc paper was measured using a caliper to determine the antibacterial properties of FAp, CuO, and FAp-CuO [5].

3. Results and Discussion

3.1. XRD

The purpose of calcining golden snail shells at 1000°C for 6 hours is to decompose $CaCO_3$ into CaO. The resulting solid CaO was subsequently hydrated to form $Ca(OH)_2$. Solid CaO, which is reactive to water vapor in the air, easily undergoes hydration to form $Ca(OH)_2$, even at ambient temperature. The diffractogram of the obtained $Ca(OH)_2$ was compared to the reference diffraction pattern (COD 00-152-9752), revealing $Ca(OH)_2$ as the dominant phase with a diffraction peak observed at 34.05° (with a crystallinity of 81%). Analysis indicated a calcium content of 93.64% in the $Ca(OH)_2$, slightly lower than the 99% reported by Rungpin *et al.* [8]. This discrepancy is attributed to a small amount of $CaCO_3$ and CaO remaining unconverted to $Ca(OH)_2$ (Figure 1a).

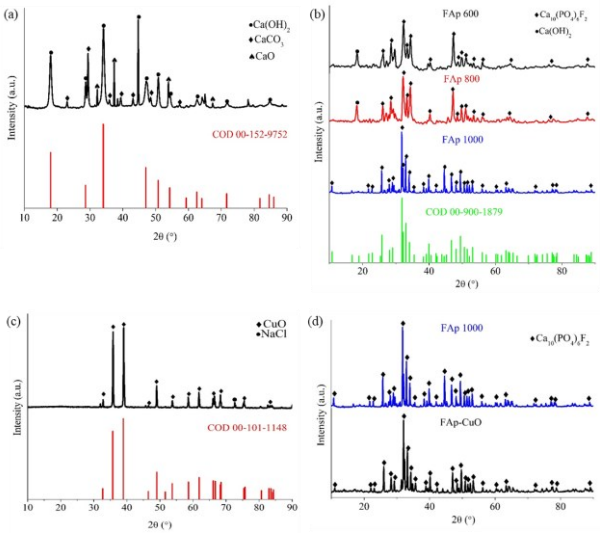

Figure 1. Diffractograms of (a) prepared $Ca(OH)_2$, (b) three FAp, (c) CuO, and (d) comparison of FAp 1000 and FAp-CuO

Table 1. Interpretation of FTIR spectrum of FAp 1000

Wavenumber (cm^{-1})		Functional group
FAp	Reference	
3469	3570 [15]	-OH
1635	1645 [5]	-OH
1418	1420 [15]	CO_3^{2-}
1043	1050 [5]	PO_4^{3-}
726	743 [5]	F^-

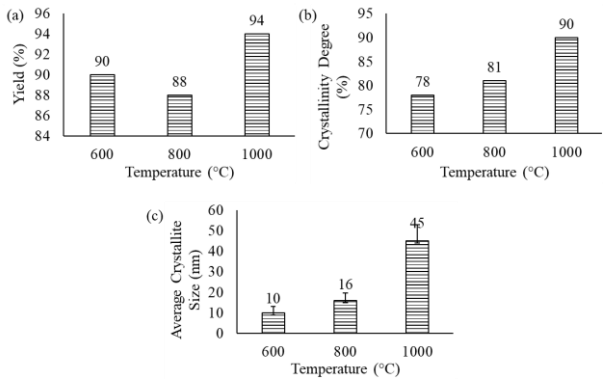

Figure 2. (a) Yield, (b) crystallinity degree, and (c) average crystallite size of the synthesized FAp after sintering at 600, 800, and 1000°C

The FAp synthesized using the sol-gel method has different yields, crystallinity degrees, and crystallite size (Figure 2). The substitution of the -OH group by F^- ions is reported to decrease solubility while enhancing density, chemical, and thermal stability due to the high electronegativity of F^- ions [3, 17]. In the FAp synthesis process, the sintering temperature is an essential factor as it can influence the crystallinity, density, and size of the resulting crystals. The crystallinity degree was calculated from the ratio between the total area of the crystalline peaks and the total area of the diffractogram, while the average crystallite size was calculated using the Scherrer equation. Fluorapatite with a sintering temperature of 1000°C (FAp 1000) shows the maximum crystallinity. The high crystallinity degree is affected by the high sintering temperature. Increasing the sintering temperature also increases the crystal density [18]. Similar results were also reported by Borkowski *et al.* [4], who stated that the crystallite size increased from 20 nm to 50 nm when treated with a temperature of 1200°C.

The diffractograms of the three FAp products show similar diffraction peaks (Figure 1b). However, FAp 600 and FAp 800 display diffraction peaks around 18°, indicating the presence of unreacted $Ca(OH)_2$. In contrast, FAp 1000 demonstrates a peak with maximum intensity at 31.78°, consistent with the reference diffractogram (COD 00-900-1879) (Figure 1b). These results also confirm that the dominant phase of each product is apatite. In addition, the elucidated FAp structure was confirmed to have a hexagonal crystal system with lattice parameter values $a = b = 9.3874$ Å and $c = 6.8920$ Å based on the reference diffractogram (Figure 3a).

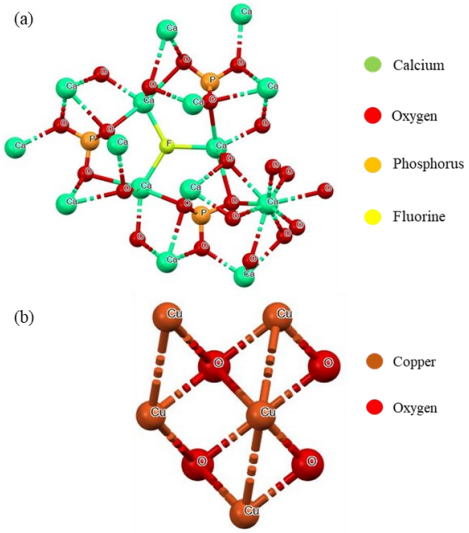

Figure 3. The structure of the elucidated (a) FAp and (b) CuO

The synthesis of CuO in this study employed two precursors: $CuCl_2.2H_2O$ and NaOH. The results indicate a yield, crystallinity degree, and average crystallite size of 84%, 58%, and 37 nm, respectively. The CuO diffractogram exhibits two prominent peaks at 35.82° and 39°, which are compared with the reference diffractogram (COD 00-101-1148), showing two prominent peaks at 35.73° and 38.93° (Figure 1c). These results confirm the successful synthesis of the CuO product, notwithstanding the presence of a NaCl byproduct (at $2\theta = 72.64°$). In addition, the elucidated CuO structure is confirmed to have a tenorite phase with a monoclinic crystal system and lattice parameter values of $a = 4.6530$ Å, $b = 3.4100$ Å, $c = 5.1080$ Å based on reference diffractogram (Figure 3b).

FAp-CuO synthesis was done by mixing FAp 1000 and CuO products in the previous step. The mole ratio between FAp and CuO is 1:1. The mole ratio value was chosen due to its ability to yield products with high crystallinity [10]. The obtained FAp-CuO diffractogram was similar to the FAp diffractogram (Figure 1d). The maximum diffraction peak of FAp-CuO is located at 32.06°, while the maximum diffraction peak of FAp is located at 31.78°. The crystallinity degree and the crystallite size of FAp-CuO are 88% and 30 nm, respectively. This value decreases when compared to only FAp. This occurs due to the replacement of Ca^{2+} ions in the FAp crystal structure by Cu^{2+} ions with a smaller ionic radius [5].

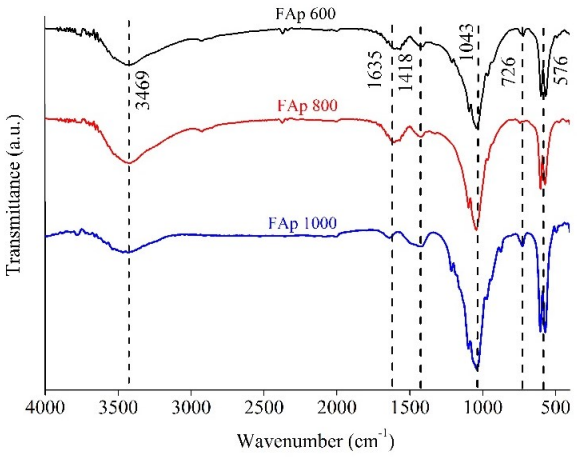

Figure 4. FTIR spectra of FAp 600, 800, and 1000

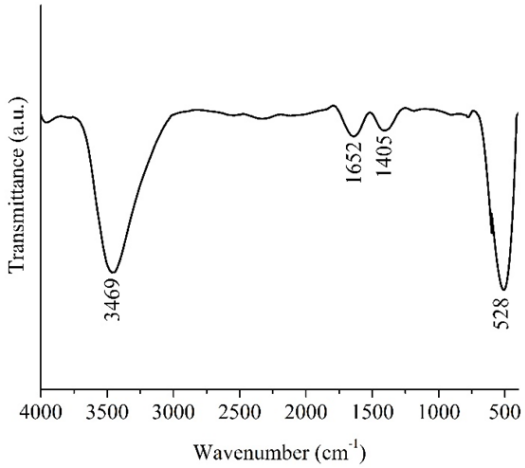

Figure 5. FTIR spectrum of CuO

3.2. FTIR

The functional groups in the three FAp samples were determined using the FTIR spectrometer, and their interpretation can be seen in Table 1. The wavenumbers 1043 and 576 cm^{-1} are the maximum absorptions from the phosphate groups (Figure 4). The presence of F^- ions in FAp gives weak absorption at wavenumber 726 cm^{-1} due to the small number of F^- ions, which is supported by the results reported by Nikonam M. *et al.* [5]. However, there are still -OH functional groups at wavenumbers 3469 and 1635 cm^{-1}. This happens because of unreacted $Ca(OH)_2$ in small amounts. In addition, there are also carbonate groups derived from $CaCO_3$, which are not maximally converted to FAp (Figure 4).

The interpretation of the FTIR spectrum and associated functional groups attributed to CuO are presented in Table 2. The absorption observed at wavenumber 528 cm^{-1} corresponds to the Cu-O bond, suggesting the formation of CuO (refer to Figure 5). Nonetheless, the presence of the -OH functional group is detected at wavenumbers 3469, 1652, and 1405 cm^{-1}. This occurrence can be attributed to incomplete drying of the CuO product or KBr pellets, resulting in the binding of water molecules [19].

The FTIR spectrum of FAp-CuO has absorption similar to those of single FAp. However, in the FTIR spectrum of FAp-CuO, no absorption was found from the -OH and CO_3^{2-} functional groups (Figure 6). The absorption at wavenumber 473 cm^{-1} comes from the Cu-O bond. In addition, the FAp-CuO FTIR spectrum experienced a shift in wavenumber values caused by the presence of Cu^{2+} ions in the FAp-CuO structure [5]. The interpretation of the FTIR spectrum obtained can be seen in Table 3.

Table 2. Interpretation of FTIR spectrum of CuO

Wavenumber (cm^{-1})		Functional group
CuO	Reference [19]	
3469	3424	-OH
1652	1631	-OH
1405	1466	-OH
528	510	Cu-O

3.3. SEM-EDX

Micrographs of SEM at 15,000 and 25,000× magnifications illustrate that the morphology of the FAp 1000 particles forms disordered agglomerations (Figure 7). This is caused by the attachment of smaller FAp particles, resulting in an overall increase in particle size [20]. In addition, agglomeration can also be caused by an increase in the surface energy of particles and the sintering temperature [21]. Elemental analysis provides information that there are five elements present in FAp, including Ca, P, F, O, and C, with different percentages (Table 4). Similar results were reported by Borkowski *et al.* [4] with atomic percentages of Ca, P, O, and F of 30.65, 15.05, 52.38, and 1.92%, respectively. The presence of carbon atoms in FAp particles is attributed to residual $CaCO_3$, which remains unconverted. Based on the obtained atomic percentage values of Ca, P, and F (Table 4), the Ca/P and P/F ratios were calculated to be 1.84 and 4.67, respectively. These values closely align with the standard ratios observed in FAp, which are typically 1.67 for Ca/P and 3.0 for P/F [22].

The surface morphology and the chemical components of FAp-CuO were analyzed using an SEM-EDX microscope. SEM images at magnifications of 15,000 and 25,000× revealed that the morphology of the agglomerated FAp-CuO particles was disorderly (Figure 7). The agglomerates formed caused the shape of the particles to be non-uniform [5]. Elemental analysis shows four elements in FAp-CuO, including Ca, P, O, and Cu, with different percentages. Notably, copper atoms exhibit the highest atomic percentage, suggesting the dominance of Cu atoms on the surface of FAp-CuO particles (Table 5). The Ca/P ratio obtained was 1.44. This decrease is attributed to the replacement of Ca^{2+} ions by Cu^{2+}, resulting in a reduction of the Ca/P ratio.

Table 3. Interpretation of FTIR spectrum of FAp-CuO

Wavenumber (cm^{-1})		Functional group
FAp-CuO	Reference [5]	
1040	1050	PO_4^{3-}
746	743	F^-
576	568	PO_4^{3-}
473	471	Cu-O

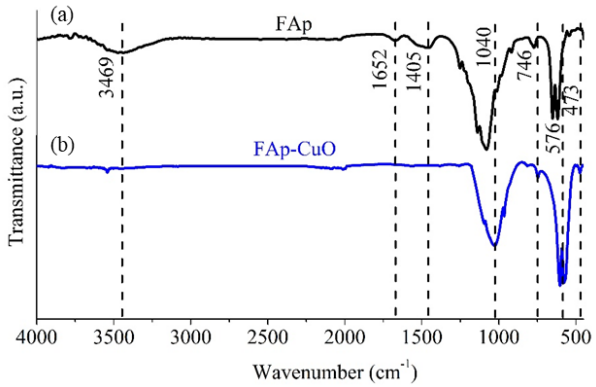

Figure 6. FTIR spectra comparison of (a) FAp and (b) FAp-CuO

3.4. Antibacterial Properties

The antibacterial test results for the FAp sample indicated the smallest average diameter of the inhibition zone compared to CuO and FAp-CuO (Table 6). This outcome is attributed to the bacteriostatic nature of the fluoride ions (F^-) released by FAp. The F^- ions released by FAp play a crucial role as chemical species essential for inhibiting bacterial growth. Fluoride ions can interfere with the performance of metabolic enzymes in bacterial cells, inhibiting the metabolism and growth of bacterial cells. In addition, bacterial cells also experience deactivation due to decreased cellular intake, which can support bacterial cell growth [11]. Similar results were also presented by Shanmugam and Gopal [10] and Nikonam M. *et al.* [5], that FAp is the sample with the lowest antibacterial properties based on the value of the inhibition zone and the percentage of reduction of bacterial cells.

CuO compound has been widely recognized as a metal oxide with excellent antibacterial properties. Selvaraj [23] reported that at a concentration of 200 ppm, CuO produced a 13 mm inhibition zone. Dadi *et al.* [24] also reported similar results, and the inhibition zone reached a maximum value of 30 mm when the concentration of CuO was increased to 1.5 M. This result was due to the nature of Cu^{2+} as an oxidizing agent which can interact with bacterial cell components and create reactive oxygen species. Furthermore, these reactive oxygen species can induce oxidative stress, interfere with protein function, and cause damage to bacterial DNA, ultimately leading to the death of bacterial cells [24]. The 200 ppm CuO sample had a larger average inhibition zone diameter than FAp (Table 6). This happens because CuO samples are bactericidal and more effective in killing bacterial cells.

Table 4. Chemical components of FAp 1000

Element	Weight percentage (%)	Atomic percentage (%)
Ca	42.14	24.94
O	32.89	48.76
P	17.65	13.52
C	5.00	9.88
F	2.32	2.90

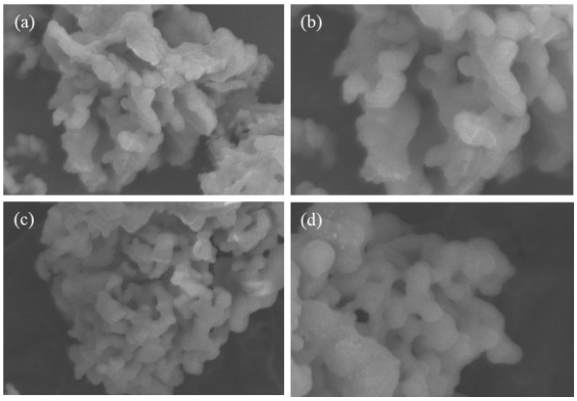

Figure 7. SEM micrographs of (a) FAp at 15,000 and (b) 25,000× magnifications, and (c) FAp-CuO with 15,000 and (d) 25,000× magnifications

Previous studies have proven that CuO and FAp-CuO can be used as Gram-positive and Gram-negative antibacterial agents. Gram-positive bacteria that are reported to be able to be inhibited by CuO include *Staphylococcus aureus* [5, 10, 24, 25], *Staphylococcus epidermidis* [13], *Bacillus thuringiensis* [26], *Bacillus cereus* [26], and *Bacillus subtilis* [23]. Gram-negative bacteria that can be inhibited include *Escherichia coli* [10, 24, 25], *Salmonella enteritidis* [13], *Pseudomonas aeruginosa* [23, 24, 26], and *Klebsiella pneumoniae* [26].

Combining CuO and FAp is one way to obtain more effective antibacterial biomaterials than single FAp and CuO. The release of Cu^{2+} and F^- ions can synergistically inhibit bacterial metabolism, growth, and nutrient intake, ultimately triggering bacterial cell death. This is supported by the larger average diameter of the FAp-CuO inhibition zone compared to the other two samples (Table 6). These results confirm that the presence of Cu^{2+} ions in FAp-CuO enhances the antibacterial properties of FAp, resulting in increased inhibition zone size and a higher reduction percentage of bacterial cells [5, 10].

The difference in results between *E. coli* and *S. aureus* is caused by the difference in the structure of the cell walls of the two bacteria. *E. coli*, classified as Gram-negative, has a thin layer of peptidoglycan on its cell wall, while *S. aureus*, classified as Gram-positive, has thicker peptidoglycan. These differences can affect the cell's response to antibacterial substances or compounds. The response of antibacterial compounds to bacteria is categorized into three groups based on the range of inhibition zone diameters, including weak (0-12 mm), medium (13-17 mm), and strong (≥ 18 mm) [27]. The small average diameter of the inhibition zones observed indicates that the three tested samples exhibited weak antibacterial activity against *E. coli* and *S. aureus*.

Table 5. Chemical components of FAp-CuO

Element	Weight percentage (%)	Atomic percentage (%)
Cu	80.42	55.73
O	13.35	36.73
Ca	4.06	4.46
P	2.17	3.09

Table 6. The average diameter of inhibition zones of FAp, CuO, and FAp-CuO

Sample	Average diameter of inhibition zones (mm)	
	E. coli ATCC 8739	*S. aureus* ATCC 6538
DMSO	0.000	0.000
FAp (0.2 mg/mL)	0.243 ± 0.046	0.000
CuO (0.2 mg/mL)	0.893 ± 0.199	0.190 ± 0.100
FAp-CuO (0.2 mg/mL)	1.397 ± 0.023	0.243 ± 0.116
Chloramphenicol	11.617 ± 0.194	10.567 ± 0.047

4. Conclusion

The sol-gel method effectively produced FAp under three distinct sintering temperature conditions. The densification process occurring at higher temperatures led to enhanced crystallinity and size of FAp crystals. Additionally, functional groups characteristic of FAp, notably PO_4^{3-} and F^-, were identified. The SEM-EDX image shows a disordered agglomeration of FAp 1000 particles with Ca/P and P/F close to standard ratios. The FTIR spectrum of CuO indicates the presence of the Cu-O group, and the diffractogram produced demonstrates that CuO is the dominating phase. The practical synthesis of FAp-CuO shows that substituting Cu^{2+} for Ca^{2+} ions can reduce crystallinity and average crystallite size. Micrographs of SEM revealed irregular aggregation on FAp-CuO particles. The antibacterial test findings demonstrated that the FAp, CuO, and FAp-CuO samples had weak antibacterial capabilities against *E. coli* and *S. aureus*, with the average diameter of the FAp-CuO inhibition zone being larger than the average diameter of single FAp and CuO.

Acknowledgment

Thanks are conveyed to Rohmat Ismail, S.Si., for its assistance in elucidating the crystal structure of FAp and CuO. Thanks were also expressed to the National Police Forensic Laboratory Center and Labotopia Indonesia for their services in XRD testing; the Materials Laboratory of Bandung Manufacturing Polytechnic for their assistance in SEM-EDX testing; and the Microbiology Laboratory, Department of Biology, IPB University for their services in antibacterial testing.

References

[1] A. J. Festas, A. Ramos, J. P. Davim, Medical devices biomaterials – A review, *Proceedings of the Institution of Mechanical Engineers, Part L: Journal of Materials: Design and Applications*, 234, 1, (2020), 218-228 https://doi.org/10.1177/1464420719882458

[2] Arie Hardian, Rosalinawati Dewi, Jasmansyah Jasmansyah, Dani Gustaman Syarif, Anceu Murniati, Synthesis and Characterization of Fe-doped Hydroxyapatite/ZnO Nanocomposites Using the Coprecipitation Method from Processed Limestone, *Jurnal Kimia Sains dan Aplikasi*, 26, 10, (2023), 404-410 https://doi.org/10.14710/jksa.26.10.404-410

[3] S. Manafi, F. Mirjalili, S. Joughehdoust, Synthesis of FAp, Forsterite, and FAp/Forsterite Nanocomposites by Sol-gel Method, *Advanced Ceramics Progress*, 6, 2, (2020), 35-42 https://doi.org/10.30501/acp.2020.109549

[4] Leszek Borkowski, Agata Przekora, Anna Belcarz, Krzysztof Palka, Grzegorz Jozefaciuk, Tomasz Lübek, Mariusz Jojczuk, Adam Nogalski, Grazyna Ginalska, Fluorapatite ceramics for bone tissue regeneration: Synthesis, characterization and assessment of biomedical potential, *Materials Science and Engineering: C*, 116, (2020), 111211 https://doi.org/10.1016/j.msec.2020.111211

[5] Raheleh Nikonam M., S. K. Sadrnezhaad, Jalil Vahdati Khaki, Effect of Cu^{2+} ion on Biological Performance of Nanostructured Fluorapatite Doped with Copper, *Scientia Iranica*, 24, 6, (2017), 2845-2855 https://doi.org/10.24200/sci.2017.4314

[6] Seyedali Seyedmajidi, Maryam Seyedmajidi, Fluorapatite: A Review of Synthesis, Properties and Medical Applications vs Hydroxyapatite, *Iranian Journal of Materials Science and Engineering*, 19, 2, (2022), 1-20 https://doi.org/10.22068/ijmse.2430

[7] Dmitry Bokov, Abduladheem Turki Jalil, Supat Chupradit, Wanich Suksatan, Mohammad Javed Ansari, Iman H. Shewael, Gabdrakhman H. Valiev, Ehsan Kianfar, Nanomaterial by Sol-Gel Method: Synthesis and Application, *Advances in Materials Science and Engineering*, 2021, (2021), 5102014 https://doi.org/10.1155/2021/5102014

[8] Nittima Rungpin, Sorapong Pavasupree, Pattarapan Prasassarakich, Sirilux Poompradub, Production of nano-calcium carbonate from shells of the freshwater channeled applesnail, *Pomacea canaliculata*, by hydrothermal treatment and its application with polyvinyl chloride, *Polymer Composites*, 36, 9, (2015), 1620-1628 https://doi.org/10.1002/pc.23070

[9] Marta Kalbarczyk, Aleksandra Szcześ, Izolda Kantor, Zoltan May, Dariusz Sternik, Synthesis and Characterization of Calcium Phosphate Materials Derived from Eggshells from Different Poultry with and without the Eggshell Membrane, *Materials*, 15, 3, (2022), 934 https://doi.org/10.3390/ma15030934

[10] Sumathi Shanmugam, Buvaneswari Gopal, Copper substituted hydroxyapatite and fluorapatite: Synthesis, characterization and antimicrobial properties, *Ceramics International*, 40, 10, Part A, (2014), 15655-15662 https://doi.org/10.1016/j.ceramint.2014.07.086

[11] Ahmed Alhilou, Thuy Do, Laith Mizban, Brian H. Clarkson, David J. Wood, Maria G. Katsikogianni, Physicochemical and Antibacterial Characterization of a Novel Fluorapatite Coating, *ACS Omega*, 1, 2, (2016), 264-276 https://doi.org/10.1021/acsomega.6b00080

[12] Thi Ha Tran, Viet Tuyen Nguyen, Copper Oxide Nanomaterials Prepared by Solution Methods, Some Properties, and Potential Applications: A Brief

Review, *International Scholarly Research Notices*, 2014, (2014), 856592 https://doi.org/10.1155/2014/856592

[13] Muhammad Imran Din, Farhan Arshad, Zaib Hussain, Maria Mukhtar, Green Adeptness in the Synthesis and Stabilization of Copper Nanoparticles: Catalytic, Antibacterial, Cytotoxicity, and Antioxidant Activities, *Nanoscale Research Letters*, 12, (2017), 638 https://doi.org/10.1186/s11671-017-2399-8

[14] Pachara Chalayon, Chanchana Tanwongsan, Antibacterial effects of copper microparticles/copper nanoparticles/copper (II) oxide nanoparticles and copper microparticles/copper nanoparticles/copper (I) oxide nanoparticles from ultrasono-electrochemical with hydrothermal assisted synthesis method, *Engineering Journal*, 25, 6, (2021), 55-66 https://doi.org/10.4186/ej.2021.25.6.55

[15] Shoaib Khan, Madiha Pirvani, Sadaf Humayoun, Omair Anjum, Saima Akram, Muhammad Asif Nathani, Synthesis of nano-hydroxyapatite and nano-fluoroapatite particles by sol-gel method, *Pakistan Journal of Medicine Dentistry*, 8, 2, (2019), 40-44

[16] Monika Patel, Sunita Mishra, Ruchi Verma, Deep Shikha, Synthesis of ZnO and CuO nanoparticles via Sol gel method and its characterization by using various technique, *Discover Materials*, 2, (2022), 1 https://doi.org/10.1007/s43939-022-00022-6

[17] Kamil Pajor, Lukasz Pajchel, Joanna Kolmas, Hydroxyapatite and Fluorapatite in Conservative Dentistry and Oral Implantology—A Review, *Materials*, 12, 17, (2019), 2683 https://doi.org/10.3390/ma12172683

[18] D. Kherifi, H. Belhouchet, S. Ramesh, K. Y. Sara Lee, A. Kenzour, S. Djoualah, M. K. G. Abbas, Y. H. Wong, S. Ramesh, Sintering behaviour of fluorapatite–silicate composites produced from natural fluorapatite and quartz, *Ceramics International*, 47, 12, (2021), 16483-16490 https://doi.org/10.1016/j.ceramint.2021.02.216

[19] Ningappa Horti, Mallappa Kamatagi, Ninganagouda Patil, Madivalagouda Sannaikar, Sanjeev Inamdar, Synthesis and optical properties of copper oxide nanoparticles: effect of solvents, *Journal of Nanophotonics*, 14, 4, (2020), 046010 https://doi.org/10.1117/1.JNP.14.046010

[20] A. Kazuz, Ž Radovanović, Dj Veljović, V. Kojić, V. Miletić, R. Petrović, Dj Janaćković, α -Tricalcium phosphate/fluorapatite based composite cements: Synthesis, mechanical properties, and biocompatibility, *Ceramics International*, 46, 16, (2020), 25149-25154 https://doi.org/10.1016/j.ceramint.2020.06.301

[21] Fariborz Sharifianjazi, Amirhossein Esmaeilkhanian, Mostafa Moradi, Amirhosein Pakseresht, Mehdi Shahedi Asl, Hassan Karimi-Maleh, Ho Won Jang, Mohammadreza Shokouhimehr, Rajender S. Varma, Biocompatibility and mechanical properties of pigeon bone waste extracted natural nano-hydroxyapatite for bone tissue engineering, *Materials Science and Engineering: B*, 264, (2021), 114950 https://doi.org/10.1016/j.mseb.2020.114950

[22] Linda Pastero, Marco Bruno, Dino Aquilano, About the Genetic Mechanisms of Apatites: A Survey on the Methodological Approaches, *Minerals*, 7, 8, (2017), 139 https://doi.org/10.3390/min7080139

[23] S. Prathap Selvaraj, Enhanced surface morphology of copper oxide (CuO) nanoparticles and its antibacterial activities, *Materials Today: Proceedings*, 50, (2022), 2865-2868 https://doi.org/10.1016/j.matpr.2020.09.574

[24] Rania Dadi, Rabah Azouani, Mamadou Traore, Christine Mielcarek, Andrei Kanaev, Antibacterial activity of ZnO and CuO nanoparticles against gram positive and gram negative strains, *Materials Science and Engineering: C*, 104, (2019), 109968 https://doi.org/10.1016/j.msec.2019.109968

[25] D. Magimai Antoni Raj, Amal George, A. Dhayal Raj, A. Albert Irudayaraj, X. Venci, J. Arumugam, S. John Sundaram, H. Joy Prabu, The role of pH in enhancing the capacity of CuO nanoparticles for antibacterial activity, *Materials Today: Proceedings*, 36, (2021), 504-508 https://doi.org/10.1016/j.matpr.2020.05.222

[26] R. Uma Maheswari, B. Jansi Rani, G. Ravi, R. Yuvakkumar, Fuad Ameen, A. Al-Sabri, Structural, morphological, optical and antibacterial properties of pentagon CuO nanoplatelets, *Journal of Sol-Gel Science and Technology*, 87, 3, (2018), 515-527 https://doi.org/10.1007/s10971-018-4773-0

[27] Clinical and Laboratory Standards Institute, *Performance Standards for Antimicrobial Susceptibility Testing*, 30th ed., 2020,